3-1-2016

HeCS-SZ: The Hectospec Survey of Sunyaev-Zeldovich-Selected Clusters

Kenneth J. Rines
Western Washington University, ken.rines@wwu.edu

Margaret J. Geller

Antonaldo Diaferio

Ho Seong Hwang

The Astrophysical Journal, 819:63 (13pp), 2016 March 1 doi:10.3847/0004-637X/819/1/63

HeCS-SZ: THE HECTOSPEC SURVEY OF SUNYAEV–ZELDOVICH-SELECTED CLUSTERS

Kenneth J. Rines[1], Margaret J. Geller[2], Antonaldo Diaferio[3,4], and Ho Seong Hwang[5]
[1] Department of Physics & Astronomy, Western Washington University, Bellingham, WA 98225, USA; kenneth.rines@wwu.edu
[2] Smithsonian Astrophysical Observatory, 60 Garden Street, Cambridge, MA 02138, USA
[3] Universita' di Torino, Dipartimento di Fisica, Torino, Italy
[4] Istituto Nazionale di Fisica Nucleare (INFN), Sezione di Torino, Torino, Italy
[5] School of Physics, Korea Institute for Advanced Study, 85 Hoegiro, Dongdaemun-Gu, 130-722 Seoul, Korea
Received 2015 July 27; accepted 2016 January 6; published 2016 February 29

ABSTRACT

We estimate cluster masses and velocity dispersions for 123 clusters from optical spectroscopy to compare the Sunyaev–Zeldovich (SZ) mass proxy and dynamical masses. Our new survey, HeCS-SZ (Hectospec Cluster Survey of SZ-selected clusters), includes 7721 new or remeasured redshifts from MMT/Hectospec observations of 21 SZ-selected clusters at redshifts $z = 0.05$–0.20. We supplement the Hectospec data with spectra from the Sloan Digital Sky Survey (SDSS) and cluster data from the Cluster Infall Regions in SDSS project and the Hectospec Cluster Survey, our Hectospec survey of clusters selected by X-ray flux. We measure the scaling relation between velocity dispersion and SZ mass estimates from the integrated Compton parameter for an SZ-complete sample of 83 clusters. The observed relation agrees very well with a simple virial scaling from mass (based on SZ) to velocity dispersion. The SZ mass estimates (calibrated with hydrostatic X-ray mass estimates) are not significantly biased compared to dynamical mass estimates under the assumption of small velocity bias of galaxies compared to dark matter particles. Significant mass bias in SZ mass estimates could relieve tension between cosmological results from *Planck* SZ cluster counts and *Planck* CMB data. In principle, SZ mass bias and velocity bias of galaxies could conspire to yield good agreement, but the required velocity bias is $\sigma_{\rm galaxy} \approx 0.77\sigma_{\rm DM}$, outside the range of recent models of velocity bias in the literature. More likely, SZ mass bias and velocity bias are both small, and the tension between SZ cluster counts and CMB data requires another explanation.

Key words: cosmology: observations – galaxies: clusters: general – galaxies: distances and redshifts – galaxies: kinematics and dynamics

Supporting material: machine-readable tables

1. INTRODUCTION

As the universe evolves, the comoving number density of clusters of fixed mass increases. The evolution of cluster abundances depends strongly on the amount of dark matter and dark energy in the universe. Thus, many groups have used different cluster mass proxies to determine the mass function and constrain cosmological parameters (e.g., Rines et al. 2007, 2008; Henry et al. 2009; Vikhlinin et al. 2009b; Mantz et al. 2010b; Rozo et al. 2010 and references therein). Recently, others have used the Sunyaev–Zeldovich (SZ) effect (Sunyaev & Zeldovich 1972) to identify large samples of clusters to constrain cosmological parameters (Benson et al. 2013; Hasselfield et al. 2013; Planck Collaboration et al. 2014a, 2014b).

Data from the *Planck* satellite show that cosmological parameters determined from anisotropies in the cosmic microwave background (CMB) disagree with those derived from cluster abundance measurements from the *Planck* SZ cluster survey (Planck Collaboration et al. 2014a, 2015a). Fewer clusters are observed than predicted by the cosmological parameters that best fit the *Planck* CMB data. Interestingly, estimates of the amplitude of structure from cosmic shear yield a similar tension with *Planck* CMB data (MacCrann et al. 2015). If SZ masses (calibrated from X-ray observations) systematically underestimate true masses by about 45%, the cosmological parameters derived from SZ cluster counts shift into agreement with the CMB results (Planck Collaboration et al. 2014a). An alternate analysis using weak lensing data for mass calibration finds no significant tension (von der Linden et al. 2014; Mantz et al. 2015), suggesting that the tension could arise from biases in the calibration of SZ masses.

Here, we compare SZ mass estimates to dynamical mass estimates based on the redshifts of cluster members. Dynamical mass estimates have a long history beginning with Zwicky (1933, 1937). In numerical simulations, either the virial theorem or the caustic technique can provide cluster mass estimates with little bias but with some intrinsic scatter due to projection effects (Diaferio 1999, hereafter refered to as D99; Evrard et al. 2008; Serra et al. 2011; Gifford & Miller 2013; Mamon et al. 2013; Old et al. 2014). Hydrodynamical simulations show that the velocity distribution of galaxies is very similar to that of dark matter particles (Faltenbacher & Diemand 2006; Lau et al. 2010), with the possible exception of the brightest few galaxies (Lau et al. 2010; Wu et al. 2013). Thus, virial masses, caustic masses, or dynamical mass proxies such as velocity dispersion are a powerful test of SZ mass estimates.

Rines et al. (2010) made the first comparison of SZ signals to mass estimates from galaxy dynamics, but the sample was limited to 15 clusters. A later study by Sifón et al. (2013) obtained optical spectroscopy for 16 SZ-selected clusters selected from observations with the Atacama Cosmology Telescope (ACT); they found that the scaling relation between SZ signal and mass (as estimated from velocity dispersions) is consistent with relations determined with other mass calibrators (X-ray, lensing). Ruel et al. (2014) measured velocity dispersions for SZ-selected clusters identified in observations with the South Pole Telescope (SPT); they conclude that

the SZ signal correlates well with velocity dispersion. The SPT results (Bocquet et al. 2015) are consistent with positive velocity bias (that is, the velocity dispersion of the galaxies is larger than the velocity dispersion of the dark matter particles). The clusters in the ACT and SPT samples span a wide range of redshifts ($0.2 < z < 1.3$). It is possible that the scaling between velocity dispersion and virial mass evolves significantly over that period. Further, the spectroscopy for these clusters is often incomplete at large radii or contains relatively few cluster members. In principle, the measured velocity dispersions could be biased (e.g., Biviano et al. 2006; Wu et al. 2013).

To provide a much broader foundation for comparison of dynamical and SZ mass proxies, we compare SZ mass estimates of 123 clusters from the *Planck* SZ catalog with velocity dispersions from wide-field optical spectroscopy. Several clusters have redshifts in the Sloan Digital Sky Survey (SDSS; Ahn et al. 2014), and many are part of the Cluster Infall Regions in SDSS project (CIRS; Rines & Diaferio 2006) or the Hectospec Cluster Survey (HeCS; Rines et al. 2013). To supplement this sample and create an SZ-selected sample of clusters, we conducted HeCS-SZ, an MMT/Hectospec spectroscopic survey of 21 clusters. We also include an analysis of 32 clusters from SDSS redshifts.

We discuss the cluster samples and spectroscopic data in Section 2. We measure the SZ-optical scaling relations in Section 3. We discuss the implications of our results in the context of other cosmological observations in Section 4. We assume a cosmology of $\Omega_m = 0.3$, $\Omega_\Lambda = 0.7$, and $H_0 = 70\,\mathrm{km\ s^{-1}\,Mpc^{-1}}$ for all calculations.

2. OBSERVATIONS

2.1. Optical Photometry and Spectroscopy

HeCS-SZ is an extension of the HeCS survey to include clusters that enable the construction of an SZ-limited sample. We measured 7721 new redshifts in 21 clusters. We combine these new measurements with the existing HeCS and CIRS surveys and with data from the literature to construct a total sample of 123 clusters. For all but a few clusters, the sampling is sufficient for a robust determination of velocity dispersion. We use SDSS photometry for all clusters.

2.1.1. Spectroscopy: CIRS and HeCS

The HeCS is a spectroscopic survey of 58 galaxy clusters at moderate redshift ($z = 0.1$–0.3) with MMT/Hectospec. HeCS includes all clusters with *ROSAT* X-ray fluxes of $f_X > 5 \times 10^{-12}\,\mathrm{erg\,s^{-1}}$ at [0.5–2.0] keV from the Bright Cluster Survey (BCS; Ebeling et al. 1998) or REFLEX survey (Böhringer et al. 2004) with optical imaging in the sixth Data Release (DR6) of SDSS (Adelman-McCarthy et al. 2008). We used DR6 photometry to select Hectospec targets. The HeCS targets are all brighter than $r = 20.8$ (SDSS catalogs are 95% complete for point sources to $r \approx 22.2$).

For HeCS, we acquired spectra with the Hectospec instrument (Fabricant et al. 2005) on the MMT 6.5 m telescope. Hectospec provides simultaneous spectroscopy of up to 300 objects across a diameter of 1°. This telescope and instrument combination is ideal for studying the virial regions and outskirts of clusters at these redshifts. Because cluster properties such as projected velocity dispersion depend on radius, wide-field spectroscopic coverage is important for measuring accurate global velocity dispersions and virial masses (Biviano et al. 2006). We used the red sequence to pre-select likely cluster members as primary targets, and we filled otherwise unassigned fibers with bluer targets (Rines et al. 2013 describes the details of target selection).

CIRS used spectroscopy from the fourth Data Release of SDSS to study the virial and infall regions of clusters. We use the dynamical data tabulated in CIRS for 25 clusters. We update dynamical parameters for two additional CIRS clusters: A2249 was poorly sampled in DR4 but has many more redshifts available in DR10. We use the DR10 redshifts to update the dynamical parameters. The central region of A2175 was poorly sampled in DR4. We thus obtained additional redshifts in the central parts of A2175 with Hectospec (see below).

2.1.2. Spectroscopy: HeCS-SZ

To mitigate against possible selection biases from the X-ray selection of the CIRS and HeCS samples, we used MMT/Hectospec to acquire new observations of 21 clusters selected from the *Planck* SZ catalog. The target clusters are in the redshift range $0.05 \leqslant z \leqslant 0.20$ and were observed mostly in order of decreasing *Planck* signal-to-noise ratio (a few clusters with relatively weak SZ signals were observed as backup targets for variable observing conditions). We also observed one field in A2175, a cluster from CIRS with limited SDSS spectroscopy in CIRS. Preliminary analysis indicated that A2175 had an unusually small velocity dispersion given its SZ mass. The additional redshifts in A2175 show that the CIRS data led to a significant underestimate of its velocity dispersion and caustic mass.

Our observing strategy closely matches that of HeCS: we used SDSS photometry to identify a red sequence in each cluster field. We then identify a cutoff in apparent magnitude that offers a good compromise of high completeness (sparser targets produce fewer fiber conflicts) and dense sampling. Targets are primarily drawn from galaxies with $g - r$ colors within 0.2 mag of the red sequence, and we assign higher priorities to brighter galaxies and galaxies closer to the cluster center. This approach provides reasonably high sampling in the cluster cores but can lead to relatively sparse sampling of dense regions outside the core. We included galaxies with slightly bluer colors (up to 0.4 mag bluer than the red sequence) as targets to fill fibers when available. We matched all targets to redshifts from the literature as compiled by NED[6] as of 2013 September as well as to SDSS DR8 spectra. Most of the targets with existing redshifts are from SDSS, but several are from targeted studies of individual clusters (e.g., Cypriano et al. 2005 for A586). Targets with existing redshifts are removed from the targeting catalogs prior to fiber assignment.

Table 1 lists 7721 new redshifts measured with Hectospec. We visually inspected all spectra to confirm the reliability of the redshift. Column 5 of Table 1 lists the cross-correlation score R_{XC} from the IRAF package *rvsao* (Kurtz & Mink 1998). A score of $R_{\mathrm{XC}} > 3$ indicates a reliable redshift; some galaxies with smaller values of R_{XC} are included when visual inspection shows multiple obvious absorption and/or emission lines and the spectrum suffers from contamination (e.g., light bleeding into the spectrum from a nearby fiber containing a bright star). Table 2 lists redshifts from SDSS and other literature (as compiled by NED) for galaxies classified as cluster members

[6] http://ned.ipac.caltech.edu

Table 1
HeCS-SZ Redshifts from MMT/Hectospec

Coordinates (J2000)		$cz_{\odot}$	σ_{cz}	R_{XC}	Flag	Member
R.A.	decl.	(km s^{-1})	(km s^{-1})			
00:09:33.60	32:31:03.16	83460	52.19	6.23	Q	0
00:09:35.55	32:14:05.00	69478	182.17	1.64	Q	0
00:09:39.32	32:21:22.38	122251	49.89	5.08	Q	0
00:09:42.73	32:16:05.45	83482	100	4.45	Q	0
00:09:43.80	32:33:54.17	108270	9.69	15.29	Q	0

(This table is available in its entirety in machine-readable form.)

Table 2
HeCS-SZ Members from Literature Redshifts

Coordinates (J2000)		$cz_{\odot}$	σ_{cz}	References
R.A.	decl.	km s^{-1}	km s^{-1}	
0:11:19.72	32:17:09.39	32168	201	2
0:11:45.24	32:24:56.17	30309	150	2
0:20:02.98	28:44:58.73	29876	27	2
0:20:05.48	28:41:01.73	29545	47	2
0:20:16.85	28:46:09.69	26793	33	2

References. (1) SDSS, (2) NED.

(This table is available in its entirety in machine-readable form.)

Table 3
HeCS-SZ Redshifts from FLWO 1.5 m/FAST

Coordinates (J2000)		$cz_{\odot}$	σ_{cz}	R_{XC}	Member
R.A.	decl.	km s^{-1}	km s^{-1}		
0:11:05.08	31:54:29.53	24574	24	9.01	0
0:11:34.79	32:28:16.28	30990	20	17.46	1
0:11:45.24	32:24:56.20	30542	51	6.47	1
0:12:27.58	32:45:09.84	12600	9	15.40	0
0:12:30.47	32:19:12.45	24565	5	31.67	0

(This table is available in its entirety in machine-readable form.)

by the caustic technique (see below). Table 3 lists 168 redshifts measured with the FAST instrument (Fabricant et al. 1998) on the 1.5 m Tillinghast telescope at the Fred Lawrence Whipple Observatory. The additional single-slit spectra from FAST reduce the incompleteness of bright (SDSS $r \lesssim 16.5$) galaxies in the HeCS-SZ clusters.

In addition, we identified several clusters in the *Planck* SZ catalog that lie below the completeness limits but that are at sufficiently low redshift ($z \lesssim 0.1$) that they have reasonable redshift coverage in SDSS DR10. We include these clusters in an extended sample.

We include four nearby ($z \leqslant 0.05$) clusters that lie inside the SDSS DR10 photometric footprint but outside the SDSS spectroscopic footprint. These nearby clusters have large numbers of redshifts available in the literature. Because of the redshift dependence of the limiting mass for SZ detection by *Planck* (driven by the large beam size of *Planck*), including these low-redshift clusters improves the sampling of low-mass clusters in the sample. The FAST redshifts in Table 3 are especially useful for these clusters.

Figure 1 shows the *Planck* SZ mass estimates versus redshift. The minimum mass a cluster must have to be detected

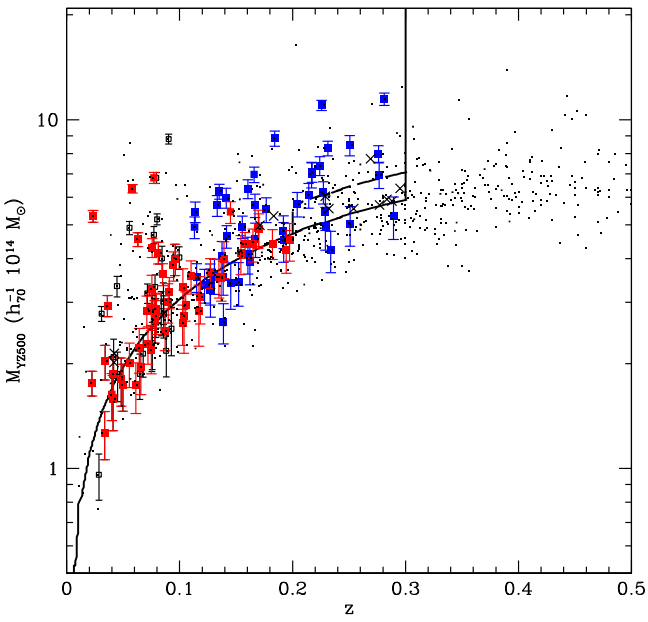

Figure 1. *Planck* SZ mass estimates vs. redshift. Open black squares show clusters with dynamical mass estimates from CIRS. Solid blue and red squares show clusters from HeCS and new HeCS-SZ clusters, respectively. Small points show the remainder of the *Planck* SZ catalog. The solid curve shows the completeness limit for the SZ catalog (80% complete for the medium-deep survey of 44% of the sky; 50% complete for the shallow survey of 56% of the sky). The clusters studied here are representative of clusters at z <0.3 in the *Planck* SZ catalog. Crosses indicate the clusters that satisfy our requirement for SDSS imaging (DR10 for $z < 0.2$, DR6 for $z = 0.2$–0.3) but that lack sufficient data for analysis. The dashed curve between $z = 0.2$ and $z = 0.3$ shows the PSZ completeness limit shifted upward by 20%.

by *Planck* increases with redshift because the SZ signal of lower mass clusters at higher redshift is diluted by the large beam below the sensitivity of *Planck*.

The CIRS and HeCS clusters provide a good sampling of the $M_{SZ} - z$ distribution, but this distribution is possibly biased due to the underlying X-ray selection of CIRS and HeCS. Figure 2 shows the X-ray luminosity of clusters in CIRS, HeCS, and HeCS-SZ as a function of redshift. The clusters we target with Hectospec include clusters that lie above the X-ray flux limits of CIRS and HeCS, but which were not in the appropriate SDSS photometric footprint, and also clusters that have X-ray fluxes below the CIRS/HeCS flux limits. Targeting these X-ray-faint clusters enables a test of the impact of X-ray selection on the scaling relation parameters based on SZ and optical properties. The X-ray luminosities are measured in the *ROSAT* band but from heterogeneous sources (Ebeling et al. 1998; Böhringer et al. 2000, 2005; Piffaretti

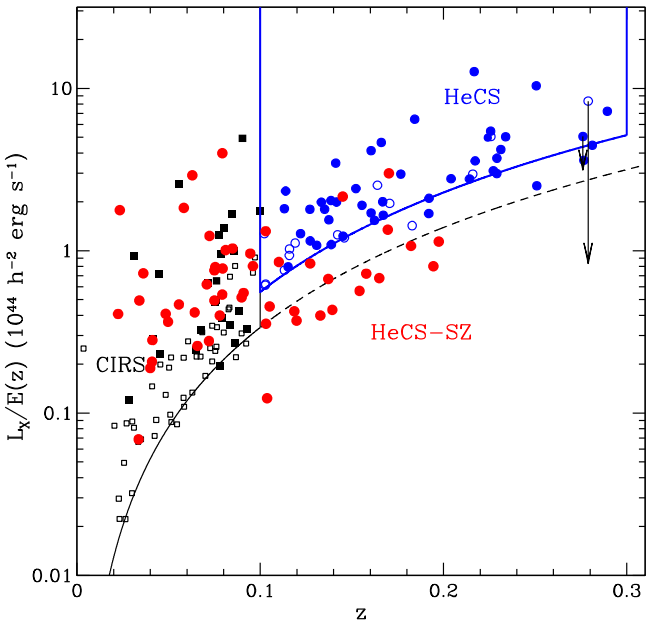

Figure 2. *ROSAT* X-ray luminosities of *Planck*-selected clusters vs. redshift. Filled symbols are clusters in the HeCS-SZ sample: black squares show clusters with dynamical mass estimates from CIRS, blue points are clusters from HeCS, and red points are new clusters in HeCS-SZ. Black and blue lines delineate the flux-limited CIRS and HeCS samples, respectively.

et al. 2011; Planck Collaboration et al. 2014b). A careful study of the X-ray properties of HeCS-SZ clusters would require a homogeneous reanalysis of *ROSAT* X-ray images.

To summarize, we base our primary analysis on a sample that is essentially SZ-complete. We call this set "Sample 1," and it includes clusters at $z < 0.3$ with SZ detections above the Planck completeness limit (Section 2.2) and Galactic latitude $|b| > 20°$ that also satisfy the following: (1) for z<0.20, imaging available in SDSS DR10; (2) for $z > 0.2$, imaging available in SDSS DR6 and X-ray flux larger than 5×10^{-12} erg s^{-1} in the *ROSAT* band (these criteria defined the HeCS sample). Note that the $z > 0.2$ clusters include 12 of the 21 clusters above the Planck completeness limit and all but 1 of the 11 clusters in the DR6 footprint with an SZ signal above 120% of the Planck completeness limit (the dashed line in Figure 1). Thus, the z >0.2 clusters comprise a nearly complete SZ-selected sample with a slightly larger completeness limit. Sample 1 includes 81 of 86 clusters above the solid and dashed curves in Figure 1. Sample 1 includes two additional clusters at $z > 0.2$.

To supplement the SZ-complete Sample 1, we also analyze an extended set of clusters we refer to as "Sample 2" that includes all Sample 1 clusters plus clusters that lie below the Planck completeness limits. Sample 2 includes new MMT/Hectospec data for five clusters in the Planck-SZ catalog.

The caustic technique (D99; Serra et al. 2011) uses a redshift-projected radius diagram to isolate cluster members from foreground and background galaxies in phase space. After smoothing the galaxy distribution in the redshift diagram, the infall regions of clusters produce well-defined envelopes containing the vast majority of cluster members. Specifically, the list of cluster members within r_{200} is 96% complete and only 2% of the members are actually interlopers; within the larger radius $3r_{200}$, where the caustic technique is the only usable method, the completeness is 95% and the interloper fraction is 8% (Serra & Diaferio 2013). The edges of this distribution are called caustics and they are related to the escape velocity profile of the cluster (see Diaferio 2009; Serra et al. 2011 for reviews). The escape velocity profile is the basis for a mass profile that can extend into the infall region where the galaxies are gravitationally bound but not virialized. Caustic mass estimates generally agree with estimates from X-ray observations and gravitational lensing (e.g., Biviano & Girardi 2003; Rines et al. 2003; Diaferio et al. 2005; Rines & Diaferio 2006; Rines et al. 2007; Geller et al. 2013, and references therein).

Figures 3–5 show the phase space diagrams of the HeCS-SZ clusters not already published in CIRS or HeCS (the poorly sampled CIRS clusters A2175 and A2249 are reproduced here with enlarged data sets). Almost all clusters display prominent infall patterns, and the caustics are shown on the figures. Clusters are ordered by decreasing SZ mass, and there is a clear trend of decreasing central velocity dispersion with decreasing SZ mass.

We apply the prescription of Danese et al. (1980) to determine the mean redshift $cz_\odot$ and projected velocity dispersion σ_p of each cluster from all galaxies within the caustics. We calculate σ_p using only the cluster members projected within r_{200} estimated from the caustic mass profile. Note that our measured velocity dispersions use the caustic technique only to define membership and the limiting radius r_{200}. Independent of its performance as a mass estimator, the caustic technique is a highly efficient membership selection algorithm, especially at the relatively small radii we focus on here (Serra & Diaferio 2013). Table 4 lists the central cluster redshifts, velocity dispersions inside r_{200}, and M_{200} from the caustic mass profile. The ninth column of Table 4 indicates whether the cluster is part of the CIRS, HeCS, or HeCS-SZ sample.

2.2. SZ Measurements

The SZ measurements are from Planck Collaboration (2014b), an all-sky SZ survey. Numerical simulations indicate that the integrated Compton y-parameter Y_{SZ} has a smaller scatter than the peak y-decrement y_{peak} (Motl et al. 2005; Planck Collaboration et al. 2014b). Planck Collaboration et al. (2014b) report only Y_{SZ}. Although y_{peak} should be nearly independent of redshift, Y_{SZ} depends on the angular size of the cluster. The quantity $Y_{SZ}D_A^2$ removes this dependence. Table 4 summarizes the *Planck* SZ measurements.

The *Planck* mass estimates are extracted from an aperture of θ_{500}, the angular radius corresponding to r_{500} (the radius r_Δ is the radius that encloses a mean density of $\Delta\rho_c(z)$ where $\rho_c(z)$ is the critical density). This radius is larger than the radii probed by some other mass estimators. For instance, Bonamente et al. (2008) and Mantz et al. (2010a) find that X-ray masses are best determined within r_{2500} (although Vikhlinin et al. 2009a and others use M_{500}). Marrone et al. (2009) uses an aperture of 350 kpc as the best match to their mass estimates from strong gravitational lensing. Because the SZ signal falls off more slowly with radius than the X-ray flux, the outer parts of clusters are more important for SZ observables than for X-ray observables. For instance, Planck Collaboration et al. (2013b) used *Planck* data to determine the average pressure profile of the intracluster medium (ICM) to radii of $3r_{500}$, a regime that is very difficult to study even with very deep *Chandra* observations. Because virial masses and velocity dispersions

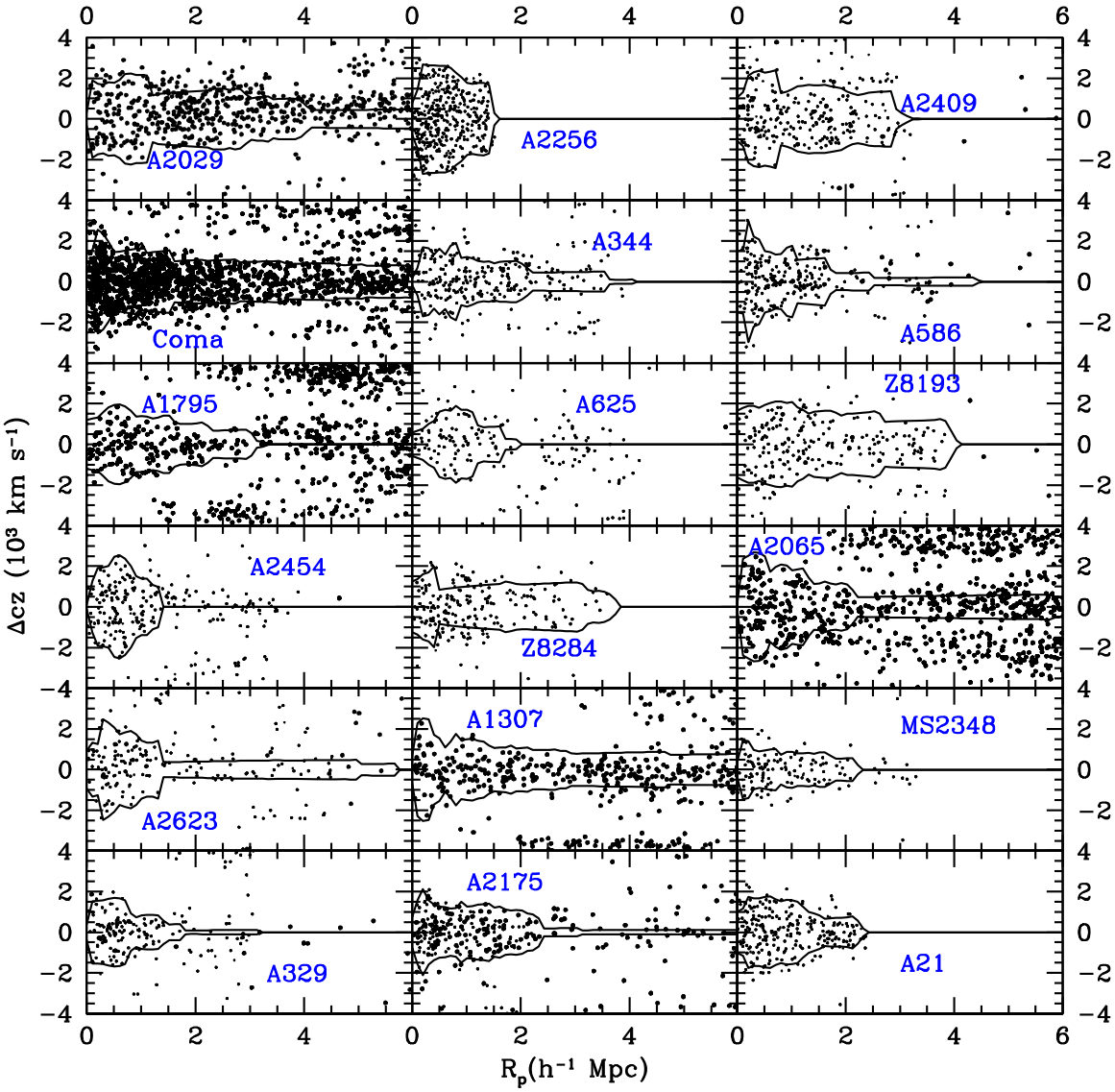

Figure 3. Redshift (rest-frame clustrocentric velocity) vs. projected radius for galaxies around HeCS-SZ clusters. The caustic pattern is evident as the trumpet-shaped regions with high density. The solid lines indicate our estimate of the location of the caustics in each cluster. Clusters are ordered left to right and top to bottom by decreasing mass as estimated from the *Planck* SZ data.

are best suited for mass estimates at radii $\sim r_{200}$, they may be better suited for comparison with SZ mass estimates.

The central redshifts in the *Planck* SZ catalog are usually close to the central redshifts we obtain in our hierarchical clustering analysis of the cluster redshifts (see D99 for details). However, for about half of the clusters, our central redshifts differ by more than a percent from the redshifts listed in the *Planck* SZ catalog. We therefore re-scale all SZ-integrated Compton parameters by $[D_A^2(z_h)/D_A^2(z_{SZ})]$, where $D_A(z_h)$ and $D_A(z_{SZ})$ are the angular diameter distances for the hierarchical center z_h and the *Planck* catalog redshift z_{SZ}. We similarly re-scale SZ mass estimates using the appropriate scaling relation from Planck Collaboration et al. (2014b).

We define an SZ-complete sample of 83 clusters from the SZ mass proxy M_{500} in the *Planck* SZ catalog (Sample 1; above the solid and dashed lines in Figure 1). The final column of Table 4 indicates whether the cluster is in Sample 1 or Sample 2. The completeness limit corresponds to the 80% completeness limit for the medium-deep survey covering 44% of the sky and to the 50% completeness limit for the shallow survey covering the remaining 56% of the sky (Planck Collaboration et al. 2014b). Our sample includes all but four clusters above this limit: two at moderate redshift (A1677 at $z = 0.18$ and A1759 at $z = 0.17$) and two at low redshift ($z \approx 0.04$: A2572 and RBS 1929). The SZ completeness limits we use are slightly above the 80% completeness limits of the updated *Planck* SZ catalog (Planck Collaboration et al. 2015b). A quick inspection shows that the updated SZ catalog contains only a few clusters above the completeness limits we use here.

3. RESULTS

3.1. Bayesian Parameter Estimation

We determine the scaling relations between SZ properties and cluster dynamics using a Bayesian approach. We define the likelihood $p(D|\theta, M)$ to be the probability of measuring the set of data D when the model M is described by the set of parameters θ; the prior $p(\theta|M)$ is the probability that the set θ

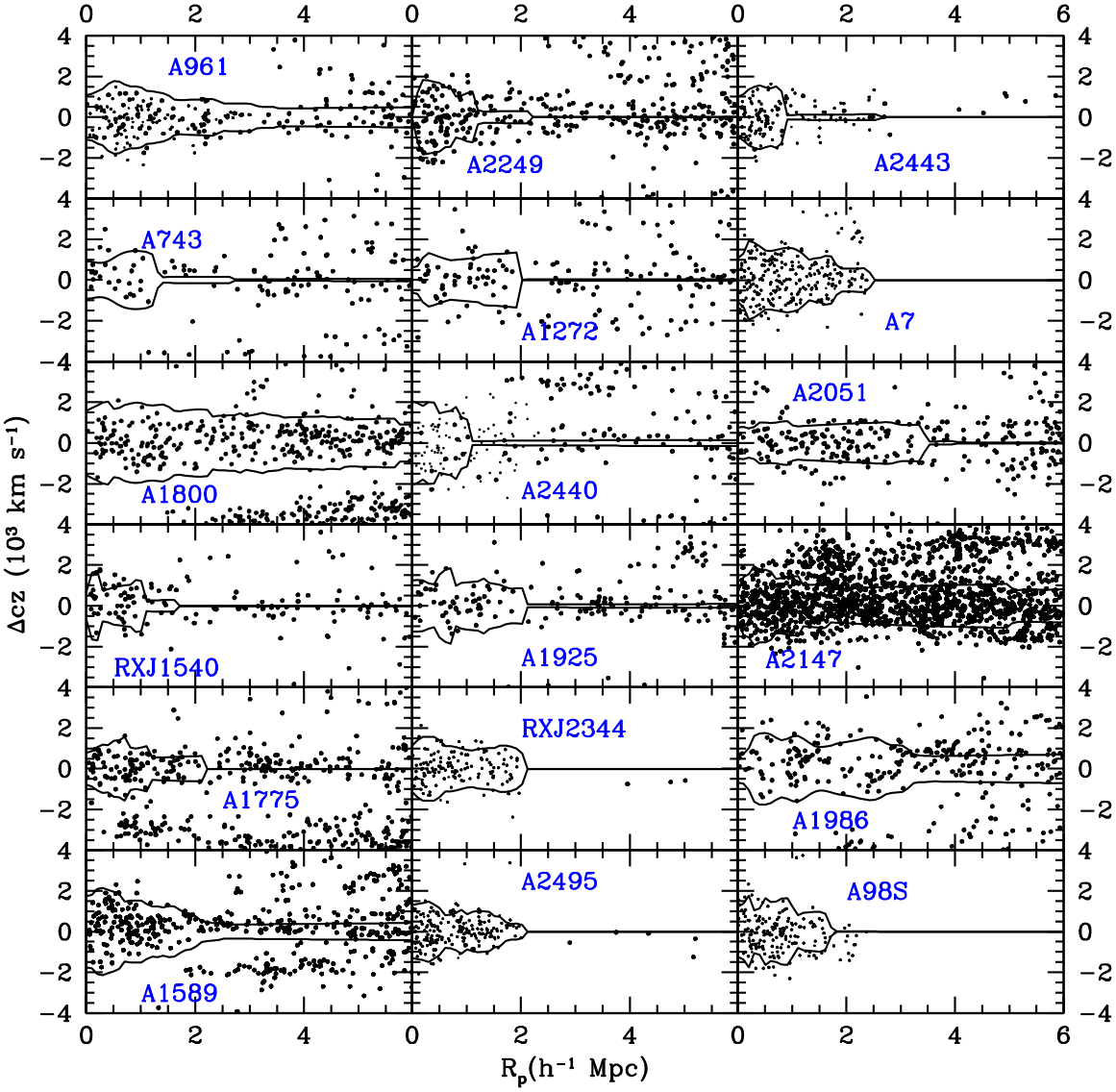

Figure 4. Same as Figure 3.

occurs. We are interested in estimating the probability density function (PDF) of the parameters θ given our data set D:

$$p(\theta|D, M) = \frac{p(D|\theta, M)p(\theta|M)}{p(D|M)}. \quad (1)$$

Given the model M, we need to assume the likelihood $p(D|\theta, M)$ and the prior $p(\theta|M)$, whereas $p(D|M)$ is a trivial normalization factor.

In this work, we are interested in describing our data with linear correlations between pairs (X,Y) of the logarithm of the observables. In general, a number of unknown hidden variables produces a scatter in the linear correlation $Y = a + bX$. We model this scatter with a single parameter, the intrinsic dispersion $\sigma_{\rm int}$. Therefore, given a measure X_i with uncertainty σ_{X_i}, the probability of measuring Y_i with uncertainty σ_{Y_i} is $p(Y_i, \sigma_{Y_i}|\theta, X_i, \sigma_{X_i})$, where $\theta = \{a, b, \sigma_{\rm int}\}$. We assume the Gaussian likelihood

$$p(D|\theta, M) = \prod_i \frac{1}{(2\pi\sigma_i^2)^{1/2}} \exp\left[\frac{-(Y_i - a - bX_i)^2}{2\sigma_i^2}\right], \quad (2)$$

where

$$\sigma_i^2 = \sigma_{\rm int}^2 + \sigma_{Y_i}^2 + b^2\sigma_{X_i}^2. \quad (3)$$

We assume independent flat priors for both a and b. For the intrinsic dispersion $\sigma_{\rm int}$, which is positively defined, we assume

$$p(\sigma_{\rm int}|M) = \frac{\mu^r}{\Gamma(r)} x^{r-1} \exp(-\mu x), \quad (4)$$

where $x = 1/\sigma_{\rm int}^2$, and $\Gamma(r)$ is the usual gamma function. This PDF describes a variate with mean r/μ, and variance r/μ^2. We set $r = \mu = 10^{-5}$, which guarantees an almost flat prior.

To estimate the parameter PDF $p(\theta|D, M)$, we perform a Markov Chain Monte Carlo (MCMC) sampling with the code APEMoST developed by Johannes Buchner and Michael Gruberbauer (Gruberbauer et al. 2009; Buchner & Gruberbauer 2011). We obtain a fairly complete sampling with 2×10^6 MCMC iterations. The boundaries of the parameter space were set to $[-100, 100]$ for a and b, and $[0.01, 100]$ for $\sigma_{\rm int}$. The initial seed of the random number generator was set with the `bash` command `GSL_RANDOM_SEED=$RANDOM`.

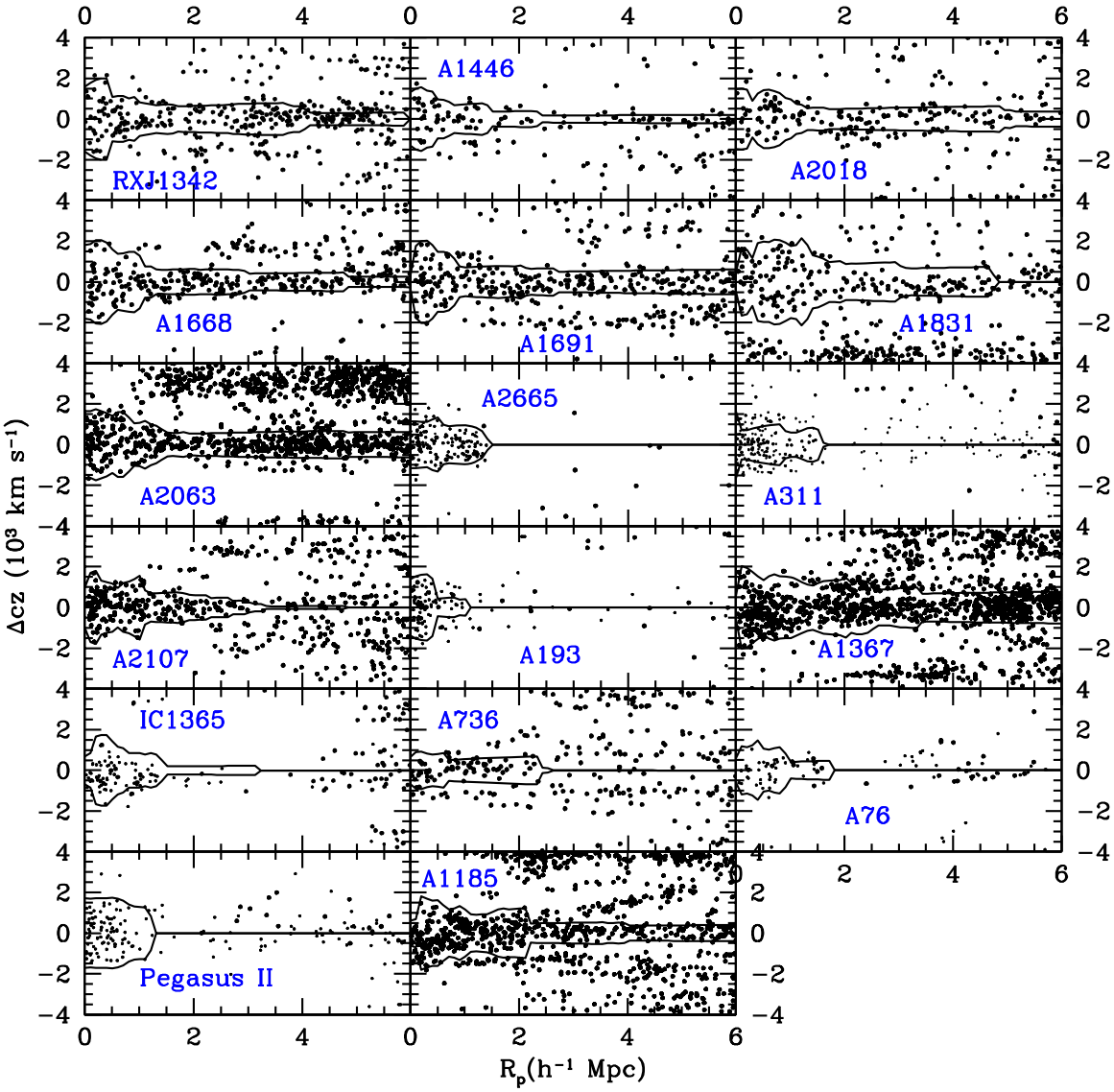

Figure 5. Same as Figure 3.

Table 4
Dynamical Masses and SZ Signals

Cluster	α (degree)	δ (degree)	z	σ_p (km s^{-1})	$M_{200,c}$ ($10^{14}M_\odot$)	M_{SZ} ($10^{14}M_\odot$)	$Y_{SZ}D_A^2$ (10^{-5} Mpc^{-2})	Spectra	*Planck* ID	Sample
A0007	2.93500	32.41700	0.10302	783^{+58}_{-48}	2.77 ± 1.14	$3.317^{+0.420}_{-0.456}$	$0.105^{+0.025}_{-0.024}$	HeCS-SZ	PSZ1G113.26-29.69	1
A0021	5.17050	28.67510	0.09456	761^{+54}_{-44}	2.92 ± 1.33	$3.825^{+0.359}_{-0.376}$	$0.146^{+0.025}_{-0.025}$	HeCS-SZ	PSZ1G114.78-33.72	1
A0076	10.00200	6.81800	0.03999	455^{+66}_{-46}	1.19 ± 0.04	$1.631^{+0.243}_{-0.258}$	$0.032^{+0.009}_{-0.008}$	HeCS-SZ	PSZ1G118.03-55.88	1
A0085	10.45870	−9.30190	0.05565	692^{+55}_{-45}	2.50 ± 1.19	$4.900^{+0.213}_{-0.217}$	$0.225^{+0.018}_{-0.018}$	CIRS	PSZ1G115.20-72.07	1
A0098S	11.61470	20.38645	0.10380	594^{+48}_{-39}	2.17 ± 0.09	$2.733^{+0.516}_{-0.591}$	$0.079^{+0.029}_{-0.028}$	HeCS-SZ	PSZ1G121.35-42.47	2

Note. Redshift z and velocity dispersion σ_p are computed for galaxies defined as members using the caustics.
(This table is available in its entirety in machine-readable form.)

As the three best-fit parameters a, b, and $\sigma_{\rm int}$ of the Bayesian analysis, we adopt the medians derived from the posterior PDF $p(\theta|D, M)$. Likewise, we adopt the boundaries of the 68% confidence levels around the medians as the uncertainties on these best-fit parameters.

3.2. Scaling Relations of SZ and Galaxy Dynamics

Figure 6 shows the relation between projected velocity dispersion σ_p and the mass M_{SZ} estimated from the *Planck* data for Sample 1 (note that for most clusters the measurements of Y_{SZ} use X-ray data to determine the region where the SZ signal

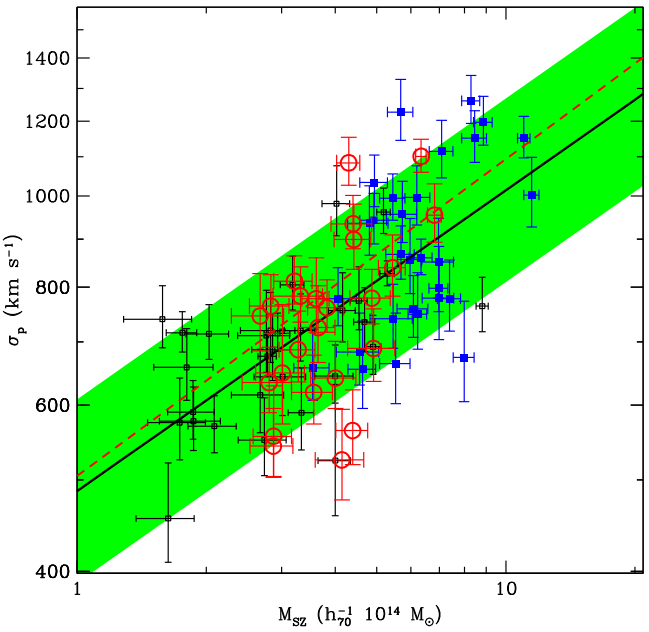

Figure 6. Scaling relation between the projected velocity dispersion σ_p and the SZ mass proxy M_{SZ} based on the integrated Compton parameter $Y_{500}D_A^2$ for clusters in the SZ-complete sample (Sample 1). The thick solid line shows the best-fit relation of $P(\sigma_p|M_{SZ})$ with the intrinsic scatter shown as the green band. Open squares, filled squares, and open circles represent clusters from CIRS, HeCS, and HeCS-SZ, respectively. The red dashed line shows the predicted relation using the virial scaling relation from Evrard et al. (2008).

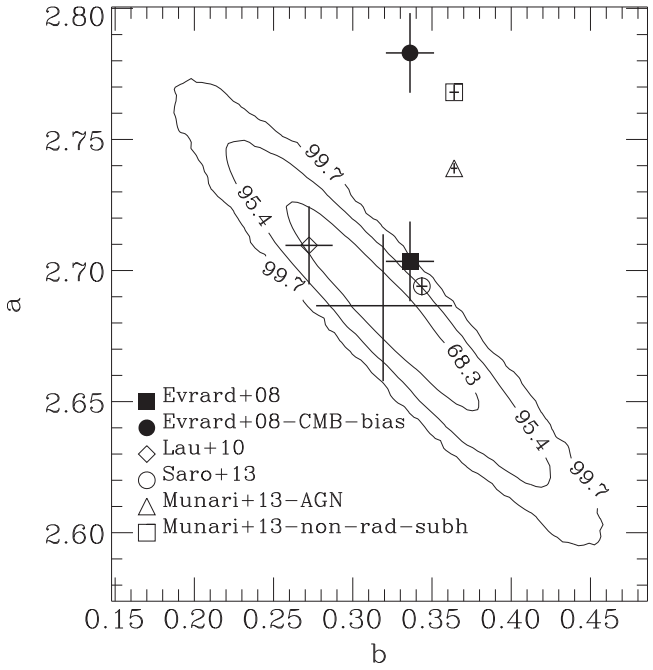

Figure 7. Parameters of the virial scaling relation between the projected velocity dispersion σ_p and the SZ mass proxy M_{SZ} based on the integrated Compton parameter $Y_{500}D_A^2$ (a is the intercept, b is the slope). Contours show confidence intervals from our Bayesian analysis and the cross without a symbol shows the median and 68% percentiles of the distribution shown with the contour levels. Points with error bars show models based on simulations. The filled square is the virial scaling relation of dark matter particles from Evrard et al. (2008). The filled circle shows this same relation re-normalized to reflect a mass bias of $b = 0.42$ (where $M_{SZ} = (1 - b)M_{true}$), the value needed to match the SZ and CMB constraints. The other points show several models of velocity bias (assuming no mass bias in M_{SZ}, i.e., $b = 0$). The open triangle and open square show the models of Munari et al. (2013) for galaxies identified from dark matter subhalos and from hydrodynamical simulations, including star formation and active galactic nucleus feedback. The open diamond shows the model of Lau et al. (2010), and the open circle shows the model of Saro et al. (2013).

is extracted). We use a Bayesian approach (see Section 3.1 for details) to determine the best-fit relation $P(\sigma_p|M_{SZ})$, that is, the predicted value of σ_p at a given observed value of M_{SZ}. We allow for intrinsic scatter in σ_p that is expected to arise from the projection effects of non-spherical clusters. Our Bayesian analysis yields a relation of

$$\log_{10}(\sigma_p) = 0.319^{+0.043}_{-0.042}\log_{10}(M_{YSZ}) + 2.687^{+0.027}_{-0.029} \quad (5)$$

with σ_p in units of km s^{-1} and M_{SZ} in units of $10^{14}h_{70}^{-1}M_\odot$. The scatter in σ_p at fixed M_{SZ} is $\log_{10}\sigma = 0.0973^{+0.0094}_{-0.0085}$. Figure 6 shows this relation as a solid line. Note that we fit $P(\sigma_p|M_{SZ})$ rather than the inverse because the statistical uncertainties in M_{SZ} are smaller than the statistical uncertainties in σ_p.

The intrinsic scatter we measure corresponds to about a factor of two in the estimated mass within r_{200}. A comparison of several richness-based and dynamics-based mass estimators demonstrate similar scatter for several mass estimators based on velocity dispersions or variations of Jeans' analysis (Old et al. 2013). Thus, the scatter probably represents geometric projection effects and not our use of the caustic technique to define cluster membership.

Previous work provides an expected value for this slope. Numerical simulations of clusters with a variety of codes yield a consistent scaling relation of the mass M_{200} with velocity dispersion, $\sigma_p \propto M_{200}^{0.33}$ (Evrard et al. 2008). This slope is measured for randomly selected dark matter particles rather than galaxies, but hydrodynamical simulations suggest that velocity bias is small for large samples of cluster galaxies (Wu et al. 2013) like HeCS and CIRS (we discuss velocity bias further in Section 4.3). The slope of the scaling relation for dark matter particles in clusters agrees well with our observed $\sigma_p - M_{SZ}$ relation (Equation (1)). Figure 6 shows our data and scaling relation compared to the virial scaling of dark matter particles, and the agreement is reasonable. Figure 7 shows the marginalized probability distribution functions of the parameters of our scaling relation along with the virial scaling of dark matter particles. Figure 7 also shows the virial scaling of dark matter particles rescaled by assuming a mass bias of $b = 0.42$, where $M_{SZ} = (1 - b)M_{true}$, the mass bias required to match the SZ counts to the CMB data (Planck Collaboration et al. 2015a). Such a large mass bias is strongly disfavored by our observations.

Note that the SZ mass estimates assume self-similar evolution of the scaling relation between the integrated Compton parameter $Y_{500}D_A^2$ and M_{500}. Our fits implicitly assume self-similar evolution in SZ mass estimates. To check whether departures from self-similar evolution affect our results, we plotted the residuals in measured velocity dispersion from our best-fit relation as a function of redshift. No significant correlation is apparent, suggesting that self-similar evolution is a reasonable approximation for our sample. This conclusion differs from the conclusion of Andreon (2014), who reported significant departures from self-similar evolution when fitting Y_X and $Y_{500}D_A^2$ relations over a broader redshift range ($z < 0.45$).

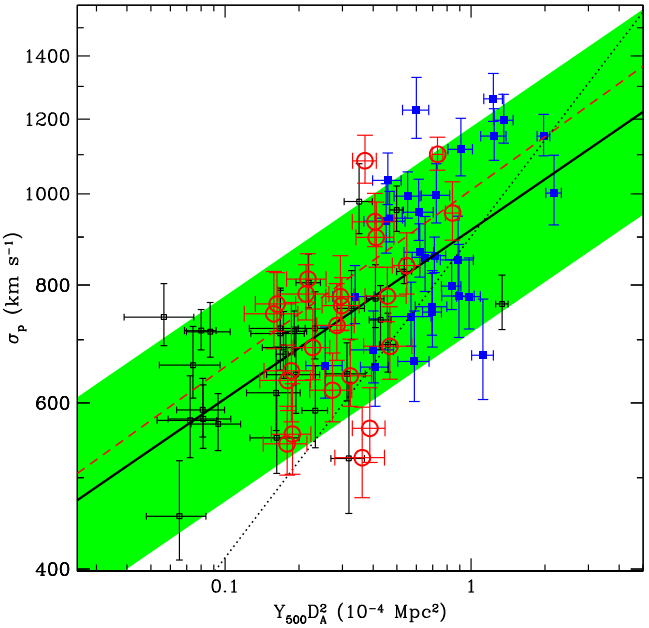

Figure 8. Similar to Figure 6 for the scaling relation between the projected velocity dispersion σ_p and the integrated Compton parameter Y_{SZ}. The dotted line shows the relation from Rines et al. (2010) from a small number of clusters. The enlarged sample we use here allows a much more robust estimate of the scaling relation.

Figure 8 shows the best-fit relation for $P(\sigma_p|Y_{SZ}D_A^2)$, the expected velocity dispersion at a fixed SZ mass proxy $Y_{SZ}D_A^2$. Planck Collaboration et al. (2014b) obtain $M_{500}^{1.79} \propto (Y_{SZ}D_A^2)$ using hydrostatic mass estimates from detailed *XMM-Newton* observations. Because the concentration-mass relation depends weakly on mass (e.g., Bullock et al. 2001), we use a fixed conversion of $M_{200} \approx 1.35M_{500}$ appropriate for concentration $c = 5$ assuming an NFW profile (Navarro et al. 1997). With these assumptions, the expected slope of the $\sigma_p - Y_{SZ}$ relation is 0.188 with an intercept of 3.003. Figure 8 shows that these values agree very well with our Bayesian analysis (see also Table 5).

In contrast with our previous work (Rines et al. 2010), the relation between the projected velocity dispersion σ_p and $Y_{SZ}D_A^2$ agrees with expectations from scaling relations of dark matter particles and simulations of the SZ effect. We attribute this difference to both the much larger (5x) sample of clusters studied here and the improved statistical methods enabled by the larger sample. As stated in Rines et al. (2010), the small sample size was insufficient to robustly determine the scaling relation due to the intrinsic scatter in the relation.

Figure 9 shows the best-fit relation $P(M_{200}|M_{SZ})$, the caustic mass M_{200} obtained at fixed M_{SZ}. The intrinsic scatter in this relation is somewhat smaller than a factor of two, consistent with the expected scatter in caustic mass estimates due to projection effects (Serra et al. 2011). Note that a similar level of scatter is found for alternate implementations of the caustic technique (Gifford & Miller 2013) as well as alternative mass estimators based on measured velocity dispersions (Old et al. 2014). While a detailed treatment of outliers is beyond the scope of this work, we note that one cluster, MS2348 +2929, with an observed velocity dispersion ≈30% smaller than predicted by its *Planck* SZ mass, is undetected in

Table 5
Scaling Relations Between Dynamical Masses and SZ Signals

Relation	b	a	σ_y
$P(\sigma_p\|Y_{500}D_A^2)$	$0.176^{+0.023}_{-0.022}$	$3.020^{+0.019}_{-0.019}$	$0.0975^{+0.0096}_{-0.0084}$
extended sample	$0.191^{+0.022}_{-0.022}$	$3.023^{+0.021}_{-0.021}$	$0.1182^{+0.0096}_{-0.0088}$
CIRS/HeCS	$0.175^{+0.029}_{-0.030}$	$3.013^{+0.024}_{-0.024}$	$0.114^{+0.012}_{-0.010}$
$P(Y_{500}D_A^2\|\sigma_p)$	$2.36^{+0.31}_{-0.29}$	$-7.57^{+0.83}_{-0.91}$	$0.371^{+0.035}_{-0.031}$
extended sample	$2.02^{+0.29}_{-0.26}$	$-6.63^{+0.75}_{-0.83}$	$0.394^{+0.029}_{-0.026}$
$P(M_{200}\|M_{SZ})$	$0.73^{+0.12}_{-0.12}$	$14.053^{+0.077}_{-0.080}$	$0.279^{+0.027}_{-0.024}$
extended sample	$0.76^{+0.12}_{-0.12}$	$14.006^{+0.072}_{-0.071}$	$0.346^{+0.027}_{-0.024}$
CIRS/HeCS	$0.70^{+0.15}_{-0.15}$	$14.069^{+0.099}_{-0.096}$	$0.308^{+0.034}_{-0.029}$
$P(M_{SZ}\|M_{200})$	$1.72^{+0.57}_{-0.79}$	$-24.2^{+11.5}_{-8.3}$	$0.46^{+0.26}_{-0.19}$
$P(\sigma_p\|M_{SZ})$	$0.319^{+0.043}_{-0.041}$	$2.687^{+0.027}_{-0.029}$	$0.0973^{+0.0094}_{-0.0085}$
extended sample	$0.339^{+0.043}_{-0.041}$	$2.665^{+0.025}_{-0.026}$	$0.1198^{+0.0096}_{-0.0087}$
$P(M_{SZ}\|\sigma_p)$	$1.42^{+0.16}_{-0.19}$	$-3.47^{+0.55}_{-0.47}$	$0.205^{+0.019}_{-0.017}$
extended sample	$1.03^{+0.12}_{-0.09}$	$-2.36^{+0.26}_{-0.34}$	$0.222^{+0.017}_{-0.015}$

Note. Fits are of the relation $P(y|x)$ assuming the linear form $\log y = a + b \log x$ with intrinsic scatter $\sigma_{\log y}$ in the relation at fixed values of $\log x$.

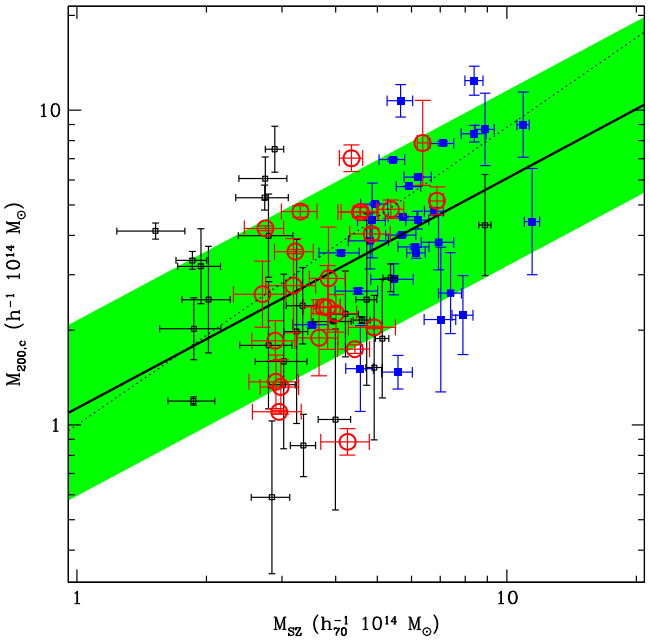

Figure 9. Similar to Figure 6 for the scaling relation between caustic mass M_{200} and M_{SZ}, the mass proxy based on the integrated Compton parameter Y_{SZ}. The dotted line shows equality (converting Hubble parameter and assuming $M_{200} = 1.35M_{500}$).

observations with the Arcminute Microkelvin Imager (Perrott et al. 2014), suggesting that the SZ mass in the *Planck* catalog is an overestimate and that a corrected SZ mass estimate would predict a velocity dispersion closer to our observed value.

Figure 10 shows the $\sigma_p - M_{SZ}$ relation for the extended sample of 123 clusters (Sample 2). There are significantly more outliers than in the SZ-complete sample. Most of these outliers have redshifts only from SDSS, and some are at $z > 0.1$. Thus, these clusters are not well sampled. Obtaining additional redshifts for these clusters could significantly alter the measured velocity dispersions (similar to the changes for the CIRS clusters A2175 and A2249 resulting from additional

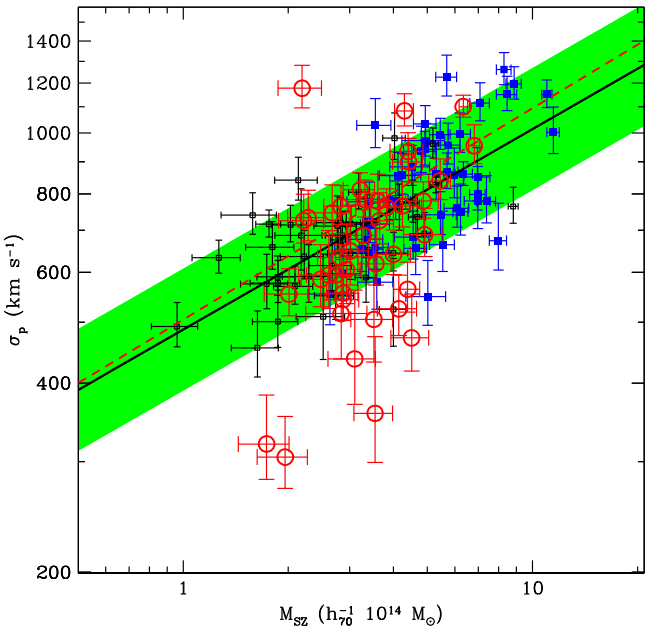

Figure 10. Scaling relation between projected velocity dispersion σ_p and the SZ mass proxy M_{SZ} based on the integrated Compton parameter $Y_{500}D_A^2$ for the extended sample (Sample 2) of *Planck*-selected clusters (including clusters below the *Planck* completeness limits). Several clusters in the extended sample are outliers below the main relation. These clusters are not well sampled in SDSS spectroscopy, so their velocity dispersions are likely underestimated.

redshift data from Hectospec and SDSS, respectively). The best-fit parameters of the scaling relation do not change significantly, but the inferred intrinsic scatter is larger due to the larger number of outliers (Table 5).

3.3. Predictor Relations

Cluster scaling relations applied to large surveys are a basis for cosmological studies, including measuring the cluster mass function or the power spectrum (Mantz et al. 2010b; Rozo et al. 2010). Andreon (2010) discusses how, given observable properties A and B, the slopes of the predictor relation $P(A|B)$ (the probability of a cluster having the property A given an observed value of property B) may be significantly different from the inverse of the slope of the predictor relation $P(B|A)$. This difference is larger when there is significant intrinsic scatter in the relation between the two properties.

Because different investigators require different predictor relations, we include here the relations between several mass observables (Table 5). We do not include constraints on the $M_{SZ} - M_{200}$ relation for the extended sample because the large scatter caused by a few outliers leads to very weak constraints on the parameters of the scaling relation.

4. DISCUSSION

4.1. Impact on the Tension Between Planck Cosmological Parameters from SZ Versus CMB

As discussed in Section 1, data from the *Planck* satellite indicate tension between cosmological parameters determined from the CMB and SZ results. One possible resolution to the tension is that the SZ mass estimates (calibrated with hydrostatic X-ray mass estimates) are biased. Comparing dynamical estimates of cluster mass from galaxy redshift surveys to the SZ mass proxies tests this hypothesis. Several studies show a strong correlation between X-ray mass estimates and SZ mass estimates (e.g., Bonamente et al. 2008; Andersson et al. 2011; Planck Collaboration et al. 2011; Czakon et al. 2015), but both methods measure the properties of the ICM. Thus, systematic effects could still be present. For instance, the ICM is likely to depart from hydrostatic equilibrium in the outer parts of the cluster (Bonamente et al. 2013). Gravitational lensing does not measure the ICM, but it does measure all of the matter along the line of sight to the cluster, introducing significant scatter into lensing mass estimates (e.g., Hoekstra et al. 2001, 2011; Hwang et al. 2014). Marrone et al. (2009) show that lensing masses are consistent with SZ estimates although with significant scatter. Recently, von der Linden et al. (2014) and Hoekstra et al. (2015) have used large samples of weak lensing mass estimates to test for systematic bias in SZ masses; both groups find that the SZ masses are systematically underestimated, but both estimates of bias are smaller than the value required to fully reconcile *Planck* CMB and SZ results (the uncertainty range in bias obtained by von der Linden et al. 2014 includes this value within the 2σ confidence interval). In contrast, Melin & Bartlett (2014) use weak lensing of the CMB to estimate cluster masses, and they find little evidence for mass bias.

As discussed in Planck Collaboration et al. (2014a), the cluster constraints are based on a scaling relation between SZ-integrated Compton decrement and X-ray masses (calculated with the assumption of hydrostatic equilibrium). They assume a hydrostatic mass bias due to non-thermal pressure support parameterized as $M_{HSE} = (1 - b)M_{true}$, where M_{true} and M_{HSE} are, respectively, the true cluster mass and the mass estimated under the assumption of hydrostatic equilibrium. Hydrodynamic simulations of intracluster gas (Nagai et al. 2007; Nelson et al. 2014) predict a value of $(1 - b) = 0.8$, and the Planck-SZ cosmological constraints are derived by allowing the bias parameter to vary in the range $0 < b < 0.3$. The tension between the SZ and CMB constraints can be eliminated by assuming that the hydrostatic mass bias is significantly larger, $(1 - b) = 0.58 \pm 0.04$ (Planck Collaboration et al. 2014a, 2015a). Note that the parameter b can have non-zero values either because of non-thermal pressure support or because of other calibration offsets (e.g., *XMM-Newton* temperature calibration; see Israel et al. 2015; Schellenberger et al. 2015).

Estimates of hydrostatic mass bias from comparisons of X-ray and lensing mass estimates find smaller offsets (e.g., Vikhlinin et al. 2009a; Mahdavi et al. 2013; Applegate et al. 2014). Recent revisions to systematic uncertainties in lensing mass estimates yield consistency in mass estimates of individual clusters between different investigators (von der Linden et al. 2014; Hoekstra et al. 2015), yielding estimates of $(1 - b) \approx 0.7 - 0.8$, intermediate between no hydrostatic mass bias and the large bias required to match CMB constraints. Alternatively, a new method of measuring the weak lensing of the CMB by clusters yields $1/(1 - b) = 0.99 \pm 0.19$, consistent with little to no mass bias (Melin & Bartlett 2014).

It is thus very interesting to see whether our dynamical mass estimates imply small hydrostatic mass bias (leaving tension between clusters and the CMB) or large hydrostatic mass bias (alleviating tension between clusters and the CMB but aggravating tension among different cluster mass estimators). As mentioned in Section 3, our best-fit scaling relation is

consistent with the predictions from the *Planck* scaling relation (based on hydrostatic mass estimates from *XMM-Newton* observations) and the $\sigma_p - M_{200}$ scaling for dark matter particles from Evrard et al. (2008). Furthermore, Figure 6 shows that renormalizing this relation by assuming a hydrostatic mass bias of $(1 - b) = 0.58 \pm 0.04$ overpredicts the velocity dispersion at fixed Y_{SZ} by an amount larger than the statistical uncertainties. That is, the CMB cosmological parameters predict significantly larger cluster velocity dispersions than our measured values.

We next consider three possible explanations of the tension between the CMB normalization of the cluster mass scale and our measurement of the relation between velocity dispersion and integrated SZ decrement. First, we investigate whether X-ray selection (used for part of the sample at larger redshift) significantly impacts the resulting scaling relation. Second, we discuss the possibility of velocity bias (galaxies moving faster or slower than dark matter particles). Third, we discuss the possible impact of massive neutrinos producing a smaller cluster abundance for a fixed matter power spectrum.

4.2. Impact of Cluster Selection

Scaling relations can be sensitive to the method of sample selection. The relation between dynamical mass and SZ signal could depend on whether the cluster sample is selected from an optical catalog, an X-ray catalog, or an SZ catalog, and whether the samples are flux-limited (detection-limited) or volume-limited. For instance, clusters with luminous cooling cores could be overrepresented in a flux-limited X-ray catalog compared to a mass-limited sample. The HeCS and CIRS cluster samples were drawn from X-ray-selected samples. Thus, all clusters from these samples have moderately large X-ray fluxes. The *Planck* early release clusters contained several that were not previously detected in X-rays. Follow up *XMM-Newton* observations of these clusters showed that they are in younger dynamical states than the rest of the early release clusters (Planck Collaboration et al. 2013a). Thus, it is conceivable that the HeCS and CIRS clusters are not a representative sample of *Planck* clusters.

We use our *Planck*-selected sample to test whether the scaling relations depend on the selection technique. Specifically, we fit the scaling relations based on only clusters from the CIRS and HeCS samples, both of which are selected by X-ray flux. There is no significant change in the best-fit parameters for the X-ray-selected sample compared to the SZ-selected sample (Table 5).[7] Thus, the impact of X-ray selection versus SZ selection appears to be small, at least for the large and complete samples that we consider here.

4.3. Can Velocity Bias Resolve the Tension?

In numerical simulations, the velocity dispersion of randomly selected dark matter particles closely traces the mass of dark matter halos (Evrard et al. 2008). Observationally, one measures the velocity dispersion of galaxies, which may move faster or slower than the underlying dark matter distribution. This "velocity bias" can be parametrized as $b_v = \sigma_{gxy}/\sigma_{DM}$, where σ_{gxy} and σ_{DM} are the velocity dispersions of galaxies and dark matter particles, respectively.

[7] Because M_{SZ} and $Y_{SZ}D_A^2$ are closely related, we do not include a separate fit for the $\sigma_p - M_{SZ}$ relation for the CIRS/HeCS subsample.

If one assumes that the *Planck* CMB cosmological parameters are correct, then the offset between the scaling relation we observe and the relation predicted by the CMB-based parameters provides information about the relation between galaxy dynamics and true cluster mass. In particular, significant negative velocity bias ($b_v \approx 0.77$) is required to bring the results into agreement.

Modeling velocity bias in simulations is a very challenging problem, due to both the uncertain physics in galaxy formation and evolution and the large dynamic range required to simulate individual cluster galaxies in a cosmological simulation. Some simulations follow the evolution of dark matter subhalos, but the evolution of galaxies may differ significantly because galaxies are expected to form at the centers of dark matter subhalos and thus survive even after their dark matter halos are tidally stripped.

Earlier, we used the consistency of the virial mass function of X-ray-selected clusters with cosmological constraints from WMAP5, supernovae, and baryon acoustic oscillations (BAOs) to conclude that velocity bias is small: $\sigma_{gxy} = (1.05 \pm 0.05)\sigma_{DM}$ (Rines et al. 2008). At present, there is no general agreement on the amount or even the sign of velocity bias, but the large negative velocity bias required for consistency with *Planck* CMB-based parameters is not predicted by any current models. Simulations suggest that small samples of cluster galaxies restricted only to the brightest members could be subject to a negative velocity bias of ~15% (Old et al. 2013; Wu et al. 2013), but these simulations also suggest that large samples such as the ones we analyze here should not be subject to significant velocity bias.

Note that a recent analysis of the redshift-space correlation function of high-mass galaxies from the SDSS Baryon Oscillation Spectroscopic Survey (BOSS) suggests that $b_v \approx 0.86$ (Guo et al. 2015b). This negative velocity bias probably reflects the fact that even massive and rich clusters contain very few high-mass galaxies (e.g., Figure 4 of Guo et al. 2015b); thus, the measured velocity bias is consistent with simulations that predict negative velocity bias for the brightest few galaxies (Old et al. 2013; Wu et al. 2013). It is also possible that the analysis of Guo et al. (2015b) does not adequately model the impact of coherent infall among satellite galaxies (Hikage & Yamamoto 2015). Again, the spectroscopic samples considered here include many galaxies below the characteristic absolute magnitude M_* and are thus expected to have smaller bias than more luminous samples. More recently, Guo et al. (2015a) performed a similar study on SDSS galaxies at low redshift. They find that the most luminous galaxies are unbiased velocity tracers, while fainter galaxies have $b_v \sim 0.85$. A full comparison of their results with ours is beyond the scope of this work.

Several recent simulations suggest that cluster galaxies should be positively biased by 5%–15% depending on the details of galaxy modeling (Lau et al. 2010; Munari et al. 2013; Saro et al. 2013). Positive velocity bias would further aggravate the tension between the velocity dispersions we measure and the large SZ-mass normalization required to match the CMB data.

Many of the simulations predict that the velocity bias depends weakly on halo mass, so a more complete description of velocity bias may require a virial scaling relation with an arbitrary slope (fixed b_v requires that the slope of the $\sigma_{gxy} - M$ relation is identical to the $\sigma_{DM} - M$ relation).

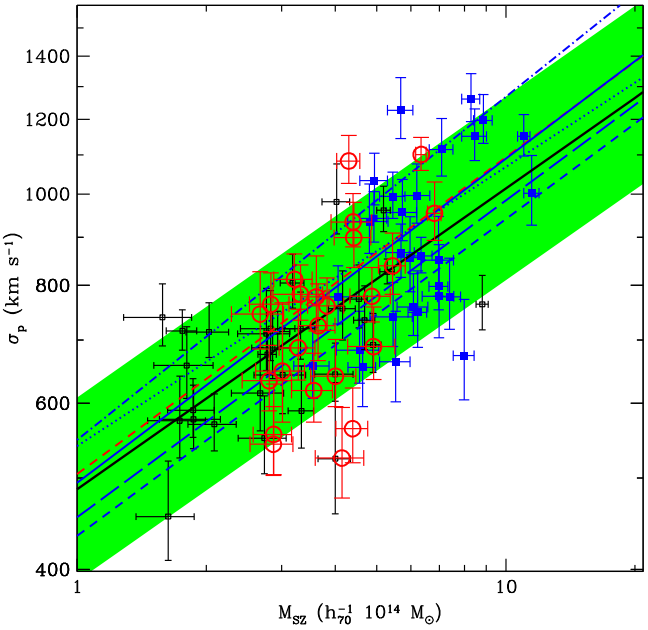

Figure 11. Scaling relation between the projected velocity dispersion σ_p and the SZ mass proxy M_{SZ} based on the integrated Compton parameter $Y_{500}D_A^2$. The thick solid line shows the best-fit relation of $P(\sigma_p|M_{SZ})$ with the intrinsic scatter shown as the green band. The other lines show several predictions of velocity bias assuming no SZ mass bias (e.g., $(1-b)=1$). The dashed–dotted line shows the prediction of Munari et al. (2013), the dotted line shows the prediction of Lau et al. (2010), the blue solid line shows the prediction of Saro et al. (2013), the long-dashed line shows the prediction from Old et al. (2013), and the blue short-dashed line shows the velocity bias for high-mass galaxies from Guo et al. (2015b).

Figure 11 shows several of these relations compared to our data, and Figure 7 shows the parameters of some of these models compared to the uncertainties in our observed scaling relation. The HeCS-SZ data and *Planck* masses are consistent with the models of Lau et al. (2010), while the models of Munari et al. (2013) lie far outside the observed relation. Importantly, although there is no consensus on the exact amount of velocity bias, none of the recent estimates are consistent with the large velocity bias ($b_v \sim 0.77$) required to reconcile the *Planck* SZ mass function with the CMB. Indeed, the discrepancy between our observed scaling relation and the models of Munari et al. (2013) is in the opposite direction of the discrepancy required to reduce the CMB-SZ tension. Specifically, adopting the CMB-based mass bias $(1-b)=0.58$ for the scaling relation of Munari et al. (2013) would produce a predicted scaling relation offset upward from the no bias prediction by the same amount as for the Evrard et al. (2008) relation: this prediction is not shown on Figure 7 because it lies above the scale of the figure.

4.4. Massive Neutrinos as a Solution?

Neutrinos with significant masses can suppress the formation of large-scale structures. Thus, massive neutrinos provide one possible explanation of the observed deficit of SZ clusters compared to the predictions from the best-fit ΛCDM model to the *Planck* CMB data. In particular, joint fits to CMB and SZ data from *Planck* yield estimates of total neutrino masses $\Sigma m_\nu = (0.40 \pm 0.21)$ eV when allowing the hydrostatic mass bias to vary between 0 and 0.3 (Planck Collaboration et al. 2014a). Adding BAO measurements yields an estimate of $\Sigma m_\nu = (0.20 \pm 0.09)$ eV (Planck Collaboration et al. 2014a). Wyman et al. (2014) point out that massive neutrinos not only alleviate tension between the *Planck* CMB results and the cluster abundance measurements, but they also alleviate tension between the *Planck* CMB results and the local measurements of the Hubble constant. Similarly, MacCrann et al. (2015) find that a similar tension exists between the *Planck* CMB results and the cosmic shear measurements; this tension can be partially alleviated with the introduction of a sterile neutrino. However, note that an alternate analysis of the cluster mass function using X-ray luminosities and weak lensing mass calibration yields reasonable agreement with the *Planck* CMB results, thus implying no need for massive neutrinos (Mantz et al. 2015). The good agreement between our measured velocity dispersions and those predicted by the *Planck* SZ masses (assuming little velocity bias) supports the mass calibration used in the *Planck* SZ analysis. Our results therefore support the possibility of massive neutrinos as a solution to the CMB-SZ tension.

Experimental measurements of neutrino oscillations place a lower limit of $\Sigma m_\nu > 0.06$ eV (95% confidence level; Capozzi et al. 2014). Constraints from the power spectrum of the Lyα forest from BOSS observations yield upper limits of $\Sigma m_\nu < 0.98$ eV, or <0.16 eV when combined with *Planck* CMB data (Palanque-Delabrouille et al. 2015). Thus, massive neutrinos remain a plausible solution to the CMB-SZ tension, but the required masses may produce tension with constraints from the Lyα forest.

5. CONCLUSIONS

The *Planck* satellite has produced a dramatic increase in the number of galaxy clusters with SZ mass estimates. Because the catalog includes many nearby clusters and covers the entire sky, many clusters in the *Planck* catalog have existing mass estimates from galaxy dynamics. Here we measure 7721 new redshifts in 21 clusters to obtain a large SZ-selected sample of 123 clusters with both dynamical and SZ mass estimates. To date, this is the largest sample of clusters used to compare velocity dispersions and SZ mass estimates. We focus on an SZ-complete sample of 83 clusters.

The measured velocity dispersions agree well with the predicted velocity dispersions from the cluster masses in the *Planck* SZ catalog and the virial scaling relation of dark matter particles. The cosmological parameters based on *Planck* CMB observations are not consistent with the mass function based on masses from the *Planck* SZ catalog. One way to resolve this tension is to allow for mass bias in the SZ masses; large mass bias ($b=0.42$ where $M_{SZ}=(1-b)M_{true}$) is required to reconcile the CMB and SZ results (Planck Collaboration et al. 2015a). Such large mass bias is strongly disfavored by our results.

In principle, velocity bias could allow galaxy velocity dispersions to agree with the virial scaling relation for dark matter particles based on strongly biased SZ masses. However, no recent estimates of the amount of velocity bias are consistent with the large velocity bias ($b_v \approx 0.77$) required for this scenario. In fact, some models of velocity bias have $b_v > 1$, a possibility that would further aggravate the tension between a possible SZ mass bias and our measured velocity dispersions.

Departures from a standard ΛCDM cosmological model could resolve the tension between CMB and SZ cosmological parameter estimates. For example, significant neutrino masses

would decrease the amplitude of the power spectrum on cluster scales relative to the normalization from the CMB (Planck Collaboration et al. 2014a). In this scenario, *Planck* cluster masses could have little bias, and the excellent agreement between the measured velocity dispersions and the virial scaling relation of dark matter particles would require that galaxy velocity bias is small (i.e., $b_v \approx 1$).

Future work on the equilibrium dynamics of cluster galaxies can test the possibility of large velocity bias: if large velocity bias is present, a Jeans analysis should reveal that the cluster masses are larger than inferred by virial scaling relations (or by the caustic technique). Future simulations of the evolution of galaxies within clusters could test whether large velocity bias is plausible. If not, our results suggest that the tension between cosmological parameters derived from CMB and SZ data may require extensions to the standard ΛCDM cosmological model. Observations of SZ-selected clusters at higher redshift could measure the evolution of cluster scaling relations and provide further insight into the origin of the CMB-SZ tension.

We thank Jim Bartlett and Nabila Aghanim for advice on using the *Planck* SZ catalogs. M.J.G. is supported by the Smithsonian Institution. A.D. acknowledges support from the grant Progetti di Ateneo/CSP TO Call2 2012 0011 "Marco Polo" of the University of Torino, the INFN grant InDark, the grant PRIN 2012 "Fisica Astroparticellare Teorica" of the Italian Ministry of University and Research. We thank Susan Tokarz for reducing the spectroscopic data and Perry Berlind and Mike Calkins for assisting with the observations. We also thank the telescope operators at the MMT and Nelson Caldwell for scheduling Hectospec queue observations.

Facilities: MMT (Hectospec), FLWO:1.5 m (FAST).

REFERENCES

Adelman-McCarthy, J. K., Agueros, M. A., Allam, S. S., et al. 2008, ApJS, 175, 297
Ahn, C. P., Alexandroff, R., Allende Prieto, C., et al. 2014, ApJS, 211, 17
Andersson, K., Benson, B. A., Ade, P. A. R., et al. 2011, ApJ, 738, 48
Andreon, S. 2010, MNRAS, 407, 263
Andreon, S. 2014, A&A, 570, L10
Applegate, D. E., von der Linden, A., Kelly, P. L., et al. 2014, MNRAS, 439, 48
Benson, B. A., de Haan, T., Dudley, J. P., et al. 2013, ApJ, 763, 147
Biviano, A., & Girardi, M. 2003, ApJ, 585, 205
Biviano, A., Murante, G., Borgani, S., et al. 2006, A&A, 456, 23
Bocquet, S., Saro, A., Mohr, J. J., et al. 2015, ApJ, 799, 214
Böhringer, H., Burwitz, V., Zhang, Y.-Y., Schuecker, P., & Nowak, N. 2005, ApJ, 633, 148
Bohringer, H., Voges, W., Huchra, J. P., et al. 2000, ApJS, 129, 435
Bohringer, H., Schuecker, P., Guzzo, L., et al. 2004, A&A, 425, 367
Bonamente, M., Joy, M., LaRoque, S. J., et al. 2008, ApJ, 675, 106
Bonamente, M., Landry, D., Maughan, B., et al. 2013, MNRAS, 428, 2812
Buchner, J., & Gruberbauer, M. 2011, APEMoST (Automated Parameter Estimation and Model Selection Toolkit), http://apemost.sourceforge.net/, commit from 2011-02-10
Bullock, J. S., Kolatt, T. S., Sigad, Y., et al. 2001, MNRAS, 321, 559
Capozzi, F., Fogli, G. L., Lisi, E., et al. 2014, PhRvD, 89, 093018
Cypriano, E. S., Lima Neto, G. B., Sodré, L., Jr., Kneib, J.-P., & Campusano, L. E. 2005, ApJ, 630, 38
Czakon, N. G., Sayers, J., Mantz, A., et al. 2015, ApJ, 806, 18
Danese, L., de Zotti, G., & di Tullio, G. 1980, A&A, 82, 322
Diaferio, A. 1999, MNRAS, 309, 610
Diaferio, A. 2009, arXiv:0901.0868
Diaferio, A., Geller, M. J., & Rines, K. J. 2005, ApJL, 628, L97
Ebeling, H., Edge, A. C., Bohringer, H., et al. 1998, MNRAS, 301, 881
Evrard, A. E., Bialek, J., Busha, M., et al. 2008, ApJ, 672, 122
Fabricant, D., Cheimets, P., Caldwell, N., & Geary, J. 1998, PASP, 110, 79
Fabricant, D., Fata, R., Roll, J., et al. 2005, PASP, 117, 1411
Faltenbacher, A., & Diemand, J. 2006, MNRAS, 369, 1698
Geller, M. J., Diaferio, A., Rines, K. J., & Serra, A. L. 2013, ApJ, 764, 58
Gifford, D., & Miller, C. J. 2013, ApJL, 768, L32
Gruberbauer, M., Kallinger, T., Weiss, W. W., & Guenther, D. B. 2009, A&A, 506, 1043
Guo, H., Zheng, Z., Zehavi, I., et al. 2015a, MNRAS, 453, 4368
Guo, H., Zheng, Z., Zehavi, I., et al. 2015b, MNRAS, 446, 578
Hasselfield, M., Hilton, M., Marriage, T. A., et al. 2013, JCAP, 7, 8
Henry, J. P., Evrard, A. E., Hoekstra, H., Babul, A., & Mahdavi, A. 2009, ApJ, 691, 1307
Hikage, C., & Yamamoto, K. 2016, MNRAS, 455, L77
Hoekstra, H., Hartlap, J., Hilbert, S., & van Uitert, E. 2011, MNRAS, 412, 2095
Hoekstra, H., Herbonnet, R., Muzzin, A., et al. 2015, MNRAS, 449, 685
Hoekstra, H., Franx, M., Kuijken, K., et al. 2001, ApJL, 548, L5
Hwang, H. S., Geller, M. J., Diaferio, A., Rines, K. J., & Zahid, H. J. 2014, ApJ, 797, 106
Israel, H., Schellenberger, G., Nevalainen, J., Massey, R., & Reiprich, T. H. 2015, MNRAS, 448, 814
Kurtz, M. J., & Mink, D. J. 1998, PASP, 110, 934
Lau, E. T., Nagai, D., & Kravtsov, A. V. 2010, ApJ, 708, 1419
MacCrann, N., Zuntz, J., Bridle, S., Jain, B., & Becker, M. R. 2015, MNRAS, 451, 2877
Mahdavi, A., Hoekstra, H., Babul, A., et al. 2013, ApJ, 767, 116
Mamon, G. A., Biviano, A., & Boué, G. 2013, MNRAS, 429, 3079
Mantz, A., Allen, S. W., Ebeling, H., Rapetti, D., & Drlica-Wagner, A. 2010a, MNRAS, 406, 1773
Mantz, A., Allen, S. W., Rapetti, D., & Ebeling, H. 2010b, MNRAS, 406, 1759
Mantz, A. B., von der Linden, A., Allen, S. W., et al. 2015, MNRAS, 446, 2205
Marrone, D. P., Smith, G. P., Richard, J., et al. 2009, ApJL, 701, L114
Melin, J.-B., & Bartlett, J. G. 2015, A&A, 578, 21
Motl, P. M., Hallman, E. J., Burns, J. O., & Norman, M. L. 2005, ApJL, 623, L63
Munari, E., Biviano, A., Borgani, S., Murante, G., & Fabjan, D. 2013, MNRAS, 430, 2638
Nagai, D., Vikhlinin, A., & Kravtsov, A. V. 2007, ApJ, 655, 98
Navarro, J. F., Frenk, C. S., & White, S. D. M. 1997, ApJ, 490, 493
Nelson, K., Lau, E. T., & Nagai, D. 2014, ApJ, 792, 25
Old, L., Gray, M. E., & Pearce, F. R. 2013, MNRAS, 434, 2606
Old, L., Skibba, R. A., Pearce, F. R., et al. 2014, MNRAS, 441, 1513
Palanque-Delabrouille, N., Yèche, C., Lesgourgues, J., et al. 2015, JCAP, 2, 45
Perrott, Y. C., Olamaie, M., Rumsey, C., et al. 2015, A&A, 580, 95
Piffaretti, R., Arnaud, M., Pratt, G. W., Pointecouteau, E., & Melin, J.-B. 2011, A&A, 534, A109
Planck Collaboration, Ade, P. A. R., Aghanim, N., et al. 2011, A&A, 536, A11
Planck Collaboration, Ade, P. A. R., Aghanim, N., et al. 2013a, A&A, 550, A130
Planck Collaboration, Ade, P. A. R., Aghanim, N., et al. 2013b, A&A, 550, A131
Planck Collaboration, Ade, P. A. R., Aghanim, N., et al. 2014a, A&A, 571, A20
Planck Collaboration, Ade, P. A. R., Aghanim, N., et al. 2014b, A&A, 571, A29
Planck Collaboration, Ade, P. A. R., Aghanim, N., et al. 2015a, arXiv:1502.01597
Planck Collaboration, Ade, P. A. R., Aghanim, N., et al. 2015b, arXiv:1502.01598
Rines, K., & Diaferio, A. 2006, AJ, 132, 1275
Rines, K., Diaferio, A., & Natarajan, P. 2007, ApJ, 657, 183
Rines, K., Diaferio, A., & Natarajan, P. 2008, ApJL, 679, L1
Rines, K., Geller, M. J., & Diaferio, A. 2010, ApJL, 715, L180
Rines, K., Geller, M. J., Diaferio, A., & Kurtz, M. J. 2013, ApJ, 767, 15
Rines, K., Geller, M. J., Kurtz, M. J., & Diaferio, A. 2003, AJ, 126, 2152
Rozo, E., Wechsler, R. H., Rykoff, E. S., et al. 2010, ApJ, 708, 645
Ruel, J., Bazin, G., Bayliss, M., et al. 2014, ApJ, 792, 45
Saro, A., Mohr, J. J., Bazin, G., & Dolag, K. 2013, ApJ, 772, 47
Schellenberger, G., Reiprich, T. H., Lovisari, L., Nevalainen, J., & David, L. 2015, A&A, 575, A30
Serra, A. L., & Diaferio, A. 2013, ApJ, 768, 116
Serra, A. L., Diaferio, A., Murante, G., & Borgani, S. 2011, MNRAS, 412, 800
Sifón, C., Menanteau, F., Hasselfield, M., et al. 2013, ApJ, 772, 25
Sunyaev, R. A., & Zeldovich, Y. B. 1972, CoASP, 4, 173
Vikhlinin, A., Burenin, R. A., Ebeling, H., et al. 2009a, ApJ, 692, 1033
Vikhlinin, A., Kravtsov, A. V., Burenin, R. A., et al. 2009b, ApJ, 692, 1060
von der Linden, A., Mantz, A., Allen, S. W., et al. 2014, MNRAS, 443, 1973
Wu, H.-Y., Hahn, O., Evrard, A. E., Wechsler, R. H., & Dolag, K. 2013, MNRAS, 436, 460
Wyman, M., Rudd, D. H., Vanderveld, R. A., & Hu, W. 2014, PhRvL, 112, 051302
Zwicky, F. 1933, AcHPh, 6, 110
Zwicky, F. 1937, ApJ, 86, 217